Environmental Research 225 (2023) 115631

Contents lists available at ScienceDirect

Environmental Research

journal homepage: www.elsevier.com/locate/envres

Regenerative marine waste towards $CaCO_3$ nanoformulation for Alzheimer's therapy

Prakashkumar Nallasamy [a], Beema shafreen Rajamohamed [b], Jeyakanthan Jeyaraman [c], Brindhadevi Kathirvel [d], Suganthy Natarajan [a,*]

[a] Bionanomaterials Research Lab, Department of Nanoscience and Technology, Alagappa University, Tamilnadu, India
[b] Department of Biotechnology, Dr. Umayal Ramanathhan College for Women, Karaikudi, Tamilnadu, India
[c] Department of Bioinformatics, Science Campus, Alagappa University, Tamilnadu, India
[d] Center for Transdisciplinary Research (CFTR), Department of Pharmacology, Saveethe Dental College, Saveetha Institute of Medical and Technical Sciences, Saveeth University, Chennai, India

ARTICLE INFO

Keywords:
Alzheimer's disease
Citronellyl acetate
$CaCO_3$ nanoparticles
$CaCO_3$ nanoformulations
Molecular docking

ABSTRACT

Alzheimer's disorder (AD) is associated with behavioural and cognitive destruction with due respect to the neurological degeneration. Conventional therapeutic approach for treatment of AD using neuroprotective drugs suffered certain limitations such as poor solubility, insufficient bioavailability, adverse side effects at higher dose and ineffective permeability on blood brain barrier (BBB). Development of nanomaterial based drug delivery system helped to overcome these barriers. Hence the present work focused on encapsulating neuroprotective drug citronellyl acetate within $CaCO_3$ nanoparticles to develop neuroprotective $CaCO_3$ nanoformulation (CA@$CaCO_3$ NFs). $CaCO_3$ was derived from marine conch shell waste, while the neuroprotective drug citronellyl acetate was scrutinized by *in-silico* high throughput screening. *In-vitro* findings revealed that CA@$CaCO_3$ nanoformulation exhibited enhanced free radical scavenging activity of 92% (IC_{50} value - 29.27 ± 2.6 μg/ml), AChE inhibition of 95% (IC_{50} value - 25.6292 ± 1.5 μg/ml) at its maximum dose (100 μg/ml). CA@$CaCO_3$ NFs attenuated the aggregation of β-amyloid peptide (Aβ) and also disaggregated the preformed mature plaques the major risk factor for AD. Overall, the present study reveals that $CaCO_3$ nanoformulations exhibits potent neuroprotective potential when compared to the $CaCO_3$ nanoparticles alone and citronellyl acetate alone due to the sustained drug release and synergistic effect of $CaCO_3$ nanoparticles and citronellyl acetate depicting the fact that $CaCO_3$ can act as promising drug delivery system for treatment of neurodegenerative and CNS related disorders.

1. Introduction

According to the World Health Organization (WHO), more than 55 million people on the globe were affected by dementia. Alzheimer's disease (AD) is the most common type of dementia, contributing to more than 70% of dementia cases leading to death over the past 3 decades (World Health Organization WHO, 2022). Alzheimer's disease is progressive neurodegenerative disorder prevalent in elderly people above the age of 60 years primarily affecting the cognitive mechanism of brain. Approximately 70% of AD is caused by genetical factors such as mutation of gene encoding for amyloid precursor protein (APP), presenilin 1 and 2, polymorphism in apolipoprotein E gene with increased presence of ε4 allele. Acquired factors like cerebrovascular disease, diabetes, hypertension, obesity and dyslipidemia have also increased risk of AD (Silva et al., 2019). Neuropathological hallmarks of AD includes oxidative stress, synaptic plaques composed of aggregated amyloid β (Aβ) peptide and neurofibrillary tangles composed of hyperphosphorylated τ-protein. Among these factors, oxidative stress (OS) directly or indirectly promotes the progression of histopathological neurodegeneration towards AD (Breijyeh and Karaman, 2020). Currently several diagnostic techniques, treatment strategies and neuroprotective drugs are available for the treatment of OS based AD. However these approaches suffered certain obstacles such as cost effectiveness, harmful electromagnetic spectrums, time lacking issues on diagnosis and poor bioavailability of drugs adverse side effects and insufficient therapeutic effect on the treatment of AD. Certain neuroprotective drugs approved by Food and Drug Administration of United States (FDA) including galantamine, donepezil and rivastigmine were

* Corresponding author.
E-mail address: suganthyn@alagappauniversity.ac.in (S. Natarajan).

https://doi.org/10.1016/j.envres.2023.115631
Received 4 January 2023; Received in revised form 4 February 2023; Accepted 4 March 2023
Available online 7 March 2023
0013-9351/

currently used for the treatment of AD which was effective only for mild AD and caused adverse side effects (Weller and Budson, 2018). Another major obstacle in the treatment of CNS related disorder is blood brain barrier permeability, which restricts the entry of therapeutic molecule in the CNS (Hussain et al., 2021). In order to overcome the drawbacks observed in AD treatment, the nanoformulations were used as an excellent alternative to achieve the neuroprotective potential. Nanoformulations were fabricated by immobilization of nutraceuticals using nanostructures such as metal, metal oxide, polymer and carbon-based materials; because the immobilization techniques contribute to the control of mobility or flow of the drug towards the targeted sites (Martín-Rapun et al., 2017). Previous reports revealed that nano encapsulated neuroprotective drugs confined excellent neuroprotective potential against AD pathogenesis (Moreno et al., 2017; Ovais et al., 2018; Saleh et al., 2021 and Prakashkumar et al., 2021).

Calcium carbonate ($CaCO_3$) a derivative composed of calcium, carbon and oxygen were available in three kinds of crystalline polymorphs such as aragonite, vaterite and calcite. Among the polymorphs, calcite is the pure and stable form of $CaCO_3$, widely used in various industrial, biological and pharmaceutical applications (Dizaj et al., 2015). $CaCO_3$ can be obtained from various biogenic sources, preferentially from shells and bones of marine species (Chavan et al., 2018; Savita et al., 2020; Hussein et al., 2020). Low cost, tunable porosity, biocompatibility, biodegradability and outstanding potential to deliver several anticancer and antimicrobial agents have promoted us in selecting $CaCO_3$ as nanocarrier for the present study (Maleki Dizaj et al., 2015; Render et al., 2016 & Trushina et al., 2022). Zhao et al. (2022) and Mailafiya et al. (2022) studied the role of $CaCO_3$ nanoparticles for the delivery of IL-12 mRNA and Curcumin for the treatment of glioblastoma and lead induced neurotoxicity under *in vivo* condition. Based on these facts, $CaCO_3$ was used as nanocarrier in the present study.

In-silico screening of essential oils was performed based on their binding affinity (in terms of scores) with progressive biomarkers of AD such as acetylcholinesterase, beta secretase and β amyloid peptide (Aβ). The above selection of the essential oil ensures its higher interactive phenomenon with AD biomarkers in order to treat the AD pathogenesis factors. Essential oil sources were selected for the present work due to its rich antioxidant behavior for combating the oxidative stress mediated neurodegeneration and its hydrophobic nature, which will facilitate its penetration into the lipophilic BBB. In addition, there are reports on use of essential oil as aroma therapeutic agent to improve cognition and moods for the treatment of AD (Scuteri et al., 2017; Benny and Thomas, 2019). Overall, this research work involves the synthesis $CaCO_3$ nanoparticles using dead damaged shells of *Chicoreus virgineusa*a marine conch species collected from Thondi, Ramanathapuram, Tamilnadu. The marine conch waste materials, which accumulate on coastal area, were mostly used for painting and decorative applications in powdered form. The present work focuses on the incorporation of marine waste derived $CaCO_3$ nanoparticles and citronellyl acetate (scrutinized based on *in-silico* high-throughput screening) as a neuroprotective nanoformulation for the treatment of AD.

2. Materials and methodology

2.1. In-silico high-throughput screening for the selection of neuroprotective drug

2.1.1. Prediction of pharmacokinetic properties

The smiles structures of the two standard drugs and seven ligands used for the present study were downloaded from Pubchem database. The pharmacokinetic properties of the ligands were evaluated by pkCSM online webserver (Pires et al., 2015).

2.1.2. Molecular docking

Ten target proteins of AD were downloaded from PDB database and the proteins were prepared before docking. Mostly the A chain of the proteins were selected for docking studies. The drug control (two) and test ligands (seven) were retrieved from pubchem database. The ligands and proteins were minimized and the intermediary steps of PDBQT files preparation suitable for docking was performed using AutoDock Tools (ADT). Further, AutoGrid was used to create the grid box for the target proteins in the respective site of binding. The parameters such as addition of hydrogen, Kollman charges and solvation were applied using ADT. The respective grid size, grid center and spacing for all the ten target proteins are shown in Table 1. AutoDock Vina was employed for docking ligand into the binding pocket of the proteins. The ligands with lowest binding affinity were extracted and aligned with the receptor for further analysis.

2.2. Reagents and sample collection

Thioflavin T, DPPH (2,2-diphenylpicrylhydrazyl), Citronellyl acetate with molecular weight 198.30 g/mol were purchased from Sigma – Aldrich. Na_2CO_3, NaOH, NaCl, HCl and chitosan were purchased from Sisco Research Laboratories Private Ltd. The dead and damaged conch shells were collected from the coastal area in Thondi, Ramanathapuram, Tamilnadu (9.74° N, 79.01° E).

2.3. Synthesis of $CaCO_3$ Nanoparticles from marine waste

The collected conch shell waste was broken into small pieces and boiled with 5% NaCl (w/v) at 150 °C for 1 h for the removal of collagen, protein, microbial entities and others from the shell surface. Conch shells were converted into $CaCO_3$ nanoparticles by step-by-step particle size reduction using the alternative strategy obtained from the combination of the traditional technique of Chavan et al. (2018) and the *in-situ* deposition technique of Hariharan et al. (2014) with few modifications. Initially, the conch shell pieces dried at 100 °C for 3 days were ground into a fine powder and the powder was further grained using planetary ball milling apparatus at 250 rpm for 1 h.An aqueous mixture consisting of 1: 3 ratio of (w/w) conch shell powder and citric acid were stirred at

Table 1
Protein targets used for the present study.

S. No	PDB ID	Protein Names	Grid Center	Grid Size
1	1P0M	Butyryl cholinesterase	x: 136.50; y: 123.28; z: 37.74	x: 39.94; y: 35.47 z: 38.53
2	2Z5X	Monoamineoxidase A(MOA-B)	x: 34.72; y: 28.12; z: -20.09	x: 36.70; y: 31.73 z: 34.98
3	3L5E	Beta Secretase (BACE)	x: 27.94; y: 5.83 z: 27.76	x: 35.75; y: 31.73 z: 33.02
4	1QXC	Beta amyloid peptide	x: 0.89; y: -1.28 z: -1.18	x: 16.56; y: 16.75 z: 17.90
5	4EY5	Acetylcholinesterase	x: -2.39; y: -40.08 z: 29.99	x: 36.70; y: 31.73 z: 34.98
6	1PBQ	NMDA receptor antagonist	x: 4.16; y: 39.39 z: -17.90	x: 33.40; y: 35.47 z: 29.74
7	1EQG	Cyclooxygenase-1 (COX-1)	x: 22.74; y: 37.63 z: 191.98	x: 43.06; y: 53.36 z: 43.30
8	1Q5K	Glycogen-synthase-kinase-3β (GSK-3β)	x: 21.38; y: 36.31 z: 3.97	x: 33.40; y: 35.47 z: 29.74
9	2FV5	TNF-α converting enzyme (TACE)	x: 1.68; y: 16.92 z: 30.90	x: 31.13; y: 30.42 z: 25.20
10	3BKL	Angiotensin converting enzyme (ACE)	x: 44.49; y: 43.98 z: 37.46	x: 35.75; y: 31.73 z: 33.02

room temperature for 12 h. The conch powder collected from the above reaction; consist of $CaCO_3$ with some traceable inorganic impurities, which were allowed to dry at 80 °C for 6 h and calcined at 750 °C for 3 h $CaCO_3$ yielded was subjected to alkaline: acidic treatment twice to remove the inorganic impurities from $CaCO_3$. $CaCO_3$ sample was stirred with 1M NaOH for 5 h followed by washing with10% HCl for several times and the yield was kept under drying and calcined at the temperature mentioned above. $CaCO_3$ nanoparticles were synthesized by *in-situ* deposition technique. For the *in-situ* deposition, the initial mixture was made of 100:1 (w/w) ratio of $CaCO_3$ dissolved in concentrated HCl and chitosan dissolved in 5% acetic acid. The reaction mixture was mixed with half the amount of Na_2CO_3 and blended, followed by heating at 50 °C for 15 min to complete blending process. Finally, the reaction was allowed to rest at RT for 12 h. The yield precipitate was washed several times with distilled water to remove the NaCl and OH^- from the $CaCO_3$. Finally, the yield was calcined at 750 °C and stored at vacuum condition until further usage.

2.4. Citronellyl acetate loading on $CaCO_3$ nanoparticles

Based on *in silico* screening, citronellyl acetate has been selected as therapeutic agent for AD therapy due to the higher binding affinity (-3.6 kcal/mol) with β amyloid peptide. In order to achieve sustained drug release, citronellyl acetate was loaded with $CaCO_3$ nanoparticles prepared from the conch shell powder by adsorption technique (Li et al., 2016). In detail, 1:1 ratio of $CaCO_3$ nanoparticles dispersed in millipore water and citronellyl acetate dissolved using 0.1% of Tween 80 was mixed together and stirred well for 30 min for better dispersion and the reaction mixture was subjected to stirring in reciprocal shaker at 150 rpm for 12 h at room temperature. Final yield was separated from the aqueous medium. Citronellyl acetate loaded $CaCO_3$ nanoformulations ($CA@CaCO_3$ NFs) were lyophilized at -80 °C and stored at vacuum condition until the usage. The percentage of yield for $CA@CaCO_3$ NFs was calculated using below formulae

$$\textbf{Yield}\ (\%) = \frac{\text{Total mass of CA@CaCO}_3\text{ NFs}}{\text{Mass of citronellyl acetate} + \text{Mass of CaCO}_3\text{ nanoparticles taken for the sythesis of CA@CaCO}_3\text{ NFs}} \times 100 \quad (1)$$

2.4.1. Drug loading efficiency

The percentage of drug loading was evaluated to determine the amount of citronellyl acetate loaded on the $CaCO_3$ nanoparticles. Briefly, the unloaded concentration of citronellyl acetate present in the supernatant collected after the fabrication of $CA@CaCO_3$ NFs was measured using UV–visible spectrophotometer at 200 nm. The slope concentration of the above supernatant with a standard calibration graph obtained for the different concentrations of citronellyl acetate (2–10 mg)provides the concentration of citronellyl acetate loaded in $CaCO_3$ nanoparticles. The percentage of drug loading was calculated using the below formulae model (Prakashkumar et al., 2021)

$$\textbf{Loading Efficiency}\ (\%) = \frac{[CA]\text{total} - [CA]\text{free}}{[CA]\text{total}} \times 100 \quad (2)$$

Whereas, [CA]total is total concentration of citronellyl acetate taken for the fabrication of $CA@CaCO_3$ NFs and [CA]free is the concentration of unloaded citronellyl acetate present in supernatant.

2.4.2. Swelling and drug release assessment

In this study, swelling and drug release profiles were assessed in the same physiological pH at 7.4 using phosphate buffered saline (PBS) as an *in-vitro* model system (Prakashkumar et al., 2021). Swelling and surface erosion of the carrier system are responsible for the release of the drug molecules and are correlated with each other. Swelling ratio was calculated by measuring the wet weight of the dry $CA@CaCO_3$ NFs added with 10 ml of PBS at room temperature for every 3 h up to 24 h.

$$\textbf{Swelling Ratio} = \frac{\text{Wet weight of CA@CaCO3 NFs} - \text{Dry weight of CA@CaCO3 NFs}}{\text{Dry weight of CA@CaCO3 NFs}} \quad (3)$$

For the evaluation of drug releasing profile, about 10 mg of $CA@CaCO_3$ NFs were added with 10 ml PBS at room temperature with standard stirring. Every 3 h up to 24 h the supernatant was collected and replaced with the equal volume of fresh PBS. The concentration of citronellyl acetate in the supernatant was measured using the standard calibration graph of citronellyl acetate from 2 mg to 10 mg using UV–Visible spectrophotometer at 200 nm. The percentage of citronellyl acetate release was calculated using below formulae

$$\textbf{Drug Release}\ (\%) = \frac{[CA]\text{released}}{[CA]\text{loaded}} \times 100 \quad (4)$$

Whereas, [CA]released is the concentration of citronellyl acetate released from the $CA@CaCO_3$ NFs in desired interval and [CA]loaded is the concentration of citronellyl acetate loaded on $CaCO_3$ nanoparticles while the fabrication of $CA@CaCO_3$ NFs.

2.5. Characterization studies

XRD (X-ray Diffraction) characterization was carried out for conch shell powder, prepared $CaCO_3$ nanoparticles and $CA@CaCO_3$ NFs for the identification of the crystallographic behavior using X-ray Diffractometer (PANalytical X'Pert PRO). UV–visible spectrophotometer (LAB INDIA, UV 3092) was majorly used in this study the specific absorbance of citronellyl acetate, $CaCO_3$ nanoparticles and $CA@CaCO_3$ NFs. Photometric mode of the UV–visible spectrophotometer was used to determine the loading and release profiles of citronellyl acetate. The FTIR (Fourier transform infra-red) spectrum at 400 to 4000 $cm^{-1}$for citronellyl acetate, $CaCO_3$ nanoparticles and $CA@CaCO_3$ NFs was obtained to predict the functional groups present in the samples using FTIR spectrometer (Bruker, Alpha II Model Advanced, Berlin, Germany). The particle size of the nanoformulations were analysed using DLS (dynamic light scattering) system (Micromeritics, Nano Plus) at 25 °C with scattering intensity of 30705 cps for the observation of particle size variation on each treatment of the $CaCO_3$ sample from the conch shell powder to $CaCO_3$ nanoparticles and $CA@CaCO_3$ NFs. Relatively, zeta potential analysis was carried out for the determination of zeta charge of $CaCO_3$ nanoparticles and $CA@CaCO_3$ NFs in suspension using Zetasizer (Ver. 8.02). SEM analysis was carried out for the morphology of the $CaCO_3$ nanoparticles alone and $CA@CaCO_3$ NFs. Along with $CaCO_3$ nanoparticles, the EDX (Energy Dispersive X-ray) spectrum has been taken for conch $CaCO_3$ to determine the difference in the elemental composition of the $CaCO_3$ samples using BRUKER Nano, GmbH, D-12489 (Germany). TEM (Transmission electron microscope) morphology and SAED (selected area electrondiffraction) patterns of $CaCO_3$ nanoparticles and $CA@CaCO_3$ NFs drop casted on copper grid were examined using High resolution transmission electron microscope (JEOL-2100+ HRTEM). ICP-OES (Inductively coupled plasma - optical emission spectrometry) analysis was carried out for the elemental prediction of marine $CaCO_3$

and $CaCO_3$ nanoparticles synthesized through step wise particle size reduction to ensure the impurities removal (PerkinElmer Optima 5300 DV, ICP - OES).

2.6. Assessment of neuroprotective potential

2.6.1. DPPH/free radical scavenging assay

Antioxidants were essential for the neuroprotection through the neutralization of oxidative stress that affects the neuronal functions. Antioxidant potential of citronellyl acetate, $CaCO_3$ nanoparticles and CA@$CaCO_3$ NFs was assessed through DPPH (2,2-diphenyl-1-picrylhydrazyl) scavenging assay. Basic principle of this assay is neutralization of free radical DPPH by accepting the proton from the antioxidant sample which is measured by the colour change from purple to yellow colour diphenylpicryl hydrazine. In brief various concentration of (10–50 μg/ml) citronellyl acetate, $CaCO_3$ nanoparticles, CA@$CaCO_3$ NFs and positive control (BHT –Butylatedhydroxytoluene (BHT) was incubated with 0.1 mM DPPH in 96 well microtitre plate under dark for 1 h for first plate and 2 h for another plate at 37 °C (Prakashkumar et al., 2020 and Prakashkumar et al., 2021). After the incubation period each plate were measured for absorbance at 517 nm against the reagent blank in the multiplate spectrophotometer (Thermo Scientific Multiskan GO, USA). The percentage of inhibition for DPPH free radicals scavenging was calculated according to the following formula

$$\textbf{DPPH Scavenging Effect}\ (\%) = \frac{\text{Absorbance of control} - \text{Absorbance of test}}{\text{Absorbance of control}} \times 100 \tag{5}$$

2.6.2. Acetylcholinesterase inhibition assay

Acetylcholinesterase (AChE) catalyzes the breakdown of acetylcholine into acetic acid and choline which plays key role in cholinergic neurotransmission. Recent reports revealed that AChE promotes Aβ fibrillization the major risk factor for neuronal death in AD and related dementia. Hence the activity of AChE was evaluated based on methodology of Ingkaninan et al. (2000). In the 96 well microtitre plate, different doses of citronellyl acetate, $CaCO_3$ nanoparticles, CA@$CaCO_3$ NFs and Donepezil (positive control) from 10 to 50 μg/ml were treated with AChE (10U/ml) in Tris-HCl (0.1M, pH – 8.0) buffer for 2 h of RT. DTNB (5,5′-dithiobis-(2-nitrobenzoic acid)) and ATCI(acetylthiocholine iodide) in the molar concentration of 0.003 M and 0.015 M respectively were added to the above assay mixture. The kinetic reaction of the AChE was initiated by the addition of ATCI and the absorbance variation of the enzyme with respect to the samples were read at 405 nm every 30 s for 3 min using multiplate reader (Thermo Scientific Multiskan GO, USA). The percentage of AChE inhibition was calculated as the rate percentage of test reaction with control reaction as follows

$$\textbf{AChE Inhibition}\ (\%) = \frac{\text{Specific activity of control} - \text{Specific activity of test}}{\text{Specific activity of control}} \times 100 \tag{6}$$

2.6.3. Amyloid beta (αβ) anti-aggregation and disaggregation studies

2.6.3.1. Aβ peptide monomer preparation. Aβ in the form of lyophilized powder was purchased from Genscript Biotech Corp. Due to the highly aggregative nature, the lyophilized powder of Aβ peptide was dissolved in HFIP ((1,1,1,3,3,3-hexafluoro-2-propanol) vortexed well and sonicated for 2 h. Then, the above reaction was lyophilized and re-dissolved using millipore water in the concentration of 1 mM at 1 mg/ml and stored at - 20 °C until the usage.

2.6.3.2. Observation of kinetic aggregation of Aβ peptide. The monomers of Aβ peptide were substantially allowed to form oligomers in Tris-HCl (pH-7.4) for 20 h. In order to evaluate the neuroprotective potential of citronellyl acetate, $CaCO_3$ nanoparticles and CA@$CaCO_3$ NFs samples against the aggregation of Aβ peptide was evaluated by treating 100 μM solution of Aβ peptide with and without the presence of the above samples at 37 °C for 96 h. From the above reaction mixture, the aliquots were taken for every 6 h and analysed for aggregation by using Thioflavin – T (Th-T) assay by two phases detailed below as phase I & phase II (Khurana et al., 2005).

2.6.3.2.1. Phase - I - Aβ peptide anti-aggregation study. In phase- I, two groups of assay mixture consisting of triplicates of 40 μg/ml of the above samples and 100 μM solution of Aβ peptide in Tris-Cl buffer pH 7.4 were incubated at 37 °C for 20 and 48 h. After incubation period the assay mixture was treated with 5 μM of Th-T prepared in Glycine-NaOH buffer at a pH of 8.5 for 10 min and the fluorescent intensity was measured using multiplate reader (Thermo Scientific Multiskan GO, USA) with the excitation and emission wavelength 450 and 485 nm respectively. Aliquots were dually diluted with 5 μM Th-T and visualised under inverted fluorescent microscope (Carl Zeiss AG, Axio Vert.A1).

2.6.3.2.2. Phase - II - Aβ peptide fibril disaggregation study. Phase II assay involves the evaluation of the disaggregation potential of citronellyl acetate, $CaCO_3$ nanoparticles and CA@$CaCO_3$ NFs samples against the matured fibrils of Aβ peptide formed by the incubation for 96h (4 days) in Tris-HCl buffer (pH – 7.4). To the matured fibrils of Aβ peptide, 40 μg/ml of the above samples were added and incubated for 9 days and the incubating mixture was subjected to Th-T staining for same spectroscopic and microscopic analysis similar to phase – I.

3. Results and discussion

3.1. In-silico high-throughput screening

3.1.1. Pharmacokinetic properties of the ligands

The pharmacokinetic properties for the ligands impose the feasibility for identification of novel drug. The ADMET efficacy of the candidate molecules were assessed using pkCSM webserver (Pires et al., 2015; Durán-Iturbide et al., 2020). Absorption property of the ligands was evaluated through CaCO-2 permeability and human intestinal absorption. Compared to the other ligands and standard drugs (Galantamine and Donepezil), Citronellyl acetate has been predicted with the good score of 1.626 and 94.9%. Similarly, for the distribution property BBB and CNS permeability was evaluated. The predicted values showed that Citronellyl acetate has 0.588 log BB value and -2.262 logPS value. The log BB value of >0.3 is considered to cross BBB and <-3 are difficult to penetrate CNS. Thus, it has been observed that Citronellyl acetate has the potential to cross BBB and CNS. Total clearance is another important pharmacokinetic property which describes the half-life and bioavailability of the drug. The predicted value of 1.538 log(mL/min/kg) determines the combination of hepatic and renal clearance. Therefore, the value obtained will be useful for dose regimen and dose size in the initial framework of *in vivo* animal and human studies. Additionally, Citronellyl acetate has been predicted to be non-toxic and non-mutagenic based on the hepatotoxicity and AMES toxicity prediction values. Thus, from the predicted properties it is determined that Citronellyl acetate as the lead molecule with good drug likeness behavior (Table 2).

3.1.2. Molecular docking

The best ligands as lead molecule were selected based on the highest binding affinity values (kcal/mol) of the docked complexes. From the molecular docking results, it was observed that Citronellyl acetate has shown the best energy values as compared to the other test ligands and standard drugs used for the study (Table 3). Additionally, the ligand has shown highest binding affinity with most of the AD targets such as NMDA, BACE, AChE and beta amyloid peptide. The binding energy of NMDA with CA is -6.2 (kcal/mol) and analysis of the NMDA-CA complex revealed that ligand is surrounded by amino acid residues including Pro124, Val181 and Phe250 through alkyl and pi-alkyl interaction. CA

Table 2
Pharmacokinetic properties of the ligands used for the study.

S. No	Ligands	Caco2	HIA (%)	BBB (log BB)	CNS (log PS)	Total Clearance (log mL)	AMES toxicity	Hepato toxicity
1	Eugenol	1.559	92.040	0.374	-2.007	0.282	Yes	No
2	Mercaptohexyl ester	1.273	93.707	0.157	-1.464	0.987	No	Yes
3	L-Ascorbic Acid	-0.255	39.154	-0.985	-3.217	0.631	No	No
4	Citronellyl acetate	1.626	94.943	0.588	-2.262	1.538	No	No
5	β-citronellol	1.489	92.83	0.627	-2.222	0.482	No	No
6	Linalool	1.493	93.163	0.598	-2.339	0.446	No	No
7	Geraniol	1.49	89.378	-0.239	-2.032	1.907	No	No
8	Galanthamine	1.594	94.994	-0.081	-2.511	0.991	No	Yes
9	Donepezil	1.273	93.707	0.157	-1.464	0.987	No	Yes

Table 3
Docking of ligands with the targets of AD.

Ligands	1EQG	1P0M	1PBQ	1Q5K	2FV5	3BKL	3L5E	4EY5	2Z5X	1QXC
Test ligands (kcal/mol)										
β-citronellol	-5.7	-5.4	-5.4	-5.4	-6.1	-5.3	-5.1	-5.9	-6.9	-3.3
Eugenol	-6.5	-6.3	-6.0	-5.7	-7.1	-5.9	-5.8	-6.4	-6.5	-3.6
Mercaptohexyl ester	-5.3	-5.2	-5.4	-4.7	-5.8	-4.6	-5.1	-5.8	-5.5	-3.2
L-Ascorbic Acid	-6.3	-5.8	-5.2	-5.0	-7.1	-5.6	-5.2	-6.2	-6.7	-3.7
Geraniol	-5.9	-5.7	-5.4	-5.6	-6.4	-5.7	-5.4	-6.3	-6.5	-3.4
Geranial	-5.7	-5.7	-6.0	-5.5	-6.4	-5.9	-5.5	-6.6	-6.4	-3.4
Linalool	-5.8	-5.3	-5.6	-5.0	-6.2	-5.2	-5.2	-6.2	-6.3	-3.5
Citronellyl acetate	-5.7	-6.0	-6.2	-5.6	-6.5	-5.8	-5.9	-7.0	-6.8	-3.6
Drugs										
Galanthamine	-7.2	-8.7	-8.1	-7.7	-6.8	-7.9	-7.9	-7.8	-8.1	-4.5
Donepezil	-8.5	-9.1	-9.1	-8.1	-9.5	-9.0	-9.3	-8.5	-10.4	-4.7

has stabilized its binding by forming hydrogen bonds with Thr124 and Arg131 amino acids of NMDA. Apart, CA also forms pi-sigma interaction with Phe92 and Trp228 and multiple vander waals (VdW) interaction with Leu125, Gln13, Asp 224, Ser 179 and Ser180. Foremost, CA has shown interaction with three amino acids (Arg131, Ser180 and Asp 224) essential for binding of glycine (Fig. 1A). Similar types of interactions are also observed with galantamine and Donepezil used as the control (Ingle and Joshi, 2017).

Interaction of CA with BACE showed binding affinity of -5.9 (kcal/mol) which was higher compared to the other test ligands. CA formed hydrogen bond with Trp137 and pi-sigma interaction with Tyr 132. The other interaction such as VdW was observed with Asp93, Ser96, Asn98, Ser97, Val130, Phe169 and Ile179 (Hassan et al., 2018). The alkyl and pi-alkyl interaction were observed with Leu91, Ile171 and Trp176 (Fig. 1B).

Molecular docking analysis revealed that CA has shown highest binding affinity of -7.0 (kcal/mol) with AChE compared to the other target protein of AD. CA has substantiated its strong binding affinity to protein by establishing two hydrogen bonds with Gly120 and Gly121. Besides, it has five pi-alkyl interactions with Trp86, Tyr124, Phe297, Phe338 and His447. Tyr86 is an important residue in the active site region for binding galantamine, which is currently used as drug for AD treatment. Amidst, CA has shown seven VdW interactions with residues of AChE. The Gly122 and Tyr133 residues of AChE showing interaction with CA are reported to interact with HuprineW and HuperzineA drugs respectively. Hence CA showing interaction with these active residues of AChE (Fig. 1C) responsible for binding of the standard drug will ease the framework of ligand as lead molecules into the drug discovery pipeline.

The binding prediction of Aβ-peptide with ligands revealed CA showed the highest binding affinity of -3.6 (kcal/mol). The analysis of poses revealed that CA shows hydrogen bond interaction with Ser26 of Aβ-peptide. Additionally, CA formed alkyl interaction with Ala30 and Ile32. Eventually, Vdw interactions were observed with CA and amino acids such as Gly25, Asn27, Ile31 and Gly33 of Aβ-peptide (Fig. 1D). Similar interaction was observed with glantamine, donepzil the control drug which showed pi-alkyl interaction with the Ala30, Ile31and Ile32 in the hydrophic pocket of Aβ-peptide (Seong et al., 2019). Thus, the results indicate that such interactions of CA with active residue of Aβ-peptide can hinder with the aggregation of the peptide during pathological condition.

3.2. Synthesis of $CaCO_3$ nanoparticles from conch waste

In this work plan, synthesis of $CaCO_3$ nanoparticles involves physical, chemical and mechanical treatments of conch shell powder, which leads to reduced particle size and increased purity of $CaCO_3$ nanoparticles. Initially, conchshell waste pieces were boiled with NaCl producing nearly white coloured pieces of conch shells due to the removal of collagen, protein, microbial entities and other impurities from the conch shell surface. Then the grounded and ball milled conch powder were calcined frequently at 750 °C after citric acid treatment, in the mid and end of 2 cycles of alkaline: acidic treatment, which significantly left the conch powder free from trace elements like Zn, Mg, Cu and other inorganic elements. Further the conch powder dissolved in concentrated HCl as calcium chloride and acetic dissolved chitosan was blended with Na_2CO_3, which acted as antacid (National Center for Biotechnology Information, 2022) to neutralize the HCl by the formation of carbonic acid and sodium hydroxide. Repeated washing removed the NaOH and other hydroxides from the above blend and calcination at 750 °C degrades the chitosan from the $CaCO_3$ powder leading to the particle size reduction of $CaCO_3$ into $CaCO_3$ nanoparticles (Hariharan et al., 2014). Synthesis of $CaCO_3$ from conch via chemical route using citric acid, NaOH, HCl treatment was based on the traditional method were conch ash was repeatedly treated with lime juice and incinerated (Chavan et al., 2018). The yield percentage of $CaCO_3$ nanoparticles derived from the conch shell powder was determined to be 84%. Reduction in percentage yield of $CaCO_3$ might be due to loss of $CaCO_3$ during citric acid treatment, acidic/alkaline treatment and in-situ deposition carried out to remove impurities in $CaCO_3$ synthesized from conch powder. Reduction in particle size of $CaCO_3$ to nanosize is due to step-by-step mechanical treatment (ball milling), chemical treatment (alkaline: acidic treatment) and in-situ deposition which was confirmed by DLS analysis

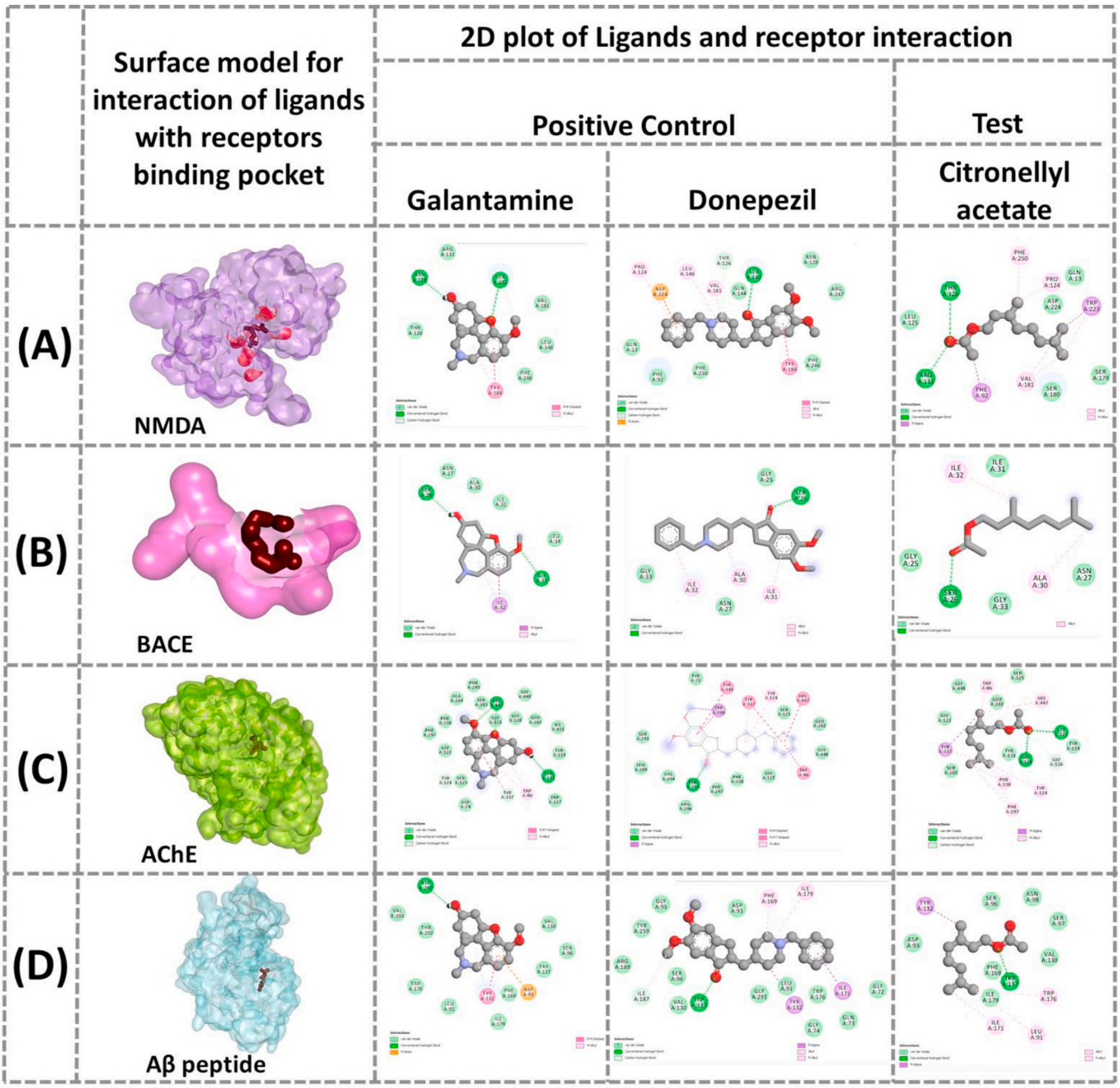

Fig. 1. Surface model of (A) NMDA, (B) BACE, (C) AChE and (D) Aβ peptide receptors showing interaction with control (Galantamine and Donepezil) and test ligand (Citronellyl acetate) and 2D plot of the Control and test ligands showing interaction with active site residues of the receptors.

3.2.1. Loading of citronellyl acetate within the $CaCO_3$NPs as CA@$CaCO_3$ NFs

Loading of citronellyl acetate within $CaCO_3$ nanoparticles as CA@$CaCO_3$ NFs was achieved by the adsorption kinetics under the process of orbital agitation. At the time of agitation, the hydrophobic drug citronellyl acetate was dissolved using 0.01% Tween 80 which gets adsorbed and loaded on the inner pore sites of $CaCO_3$ nanoparticles (Ali Said et al., 2020). The yield percentage of CA@$CaCO_3$ NFs was observed to be 93% from the 1:2 ratio (w/v) of $CaCO_3$ nanoparticles and citronellyl acetate taken for the nanoencapsulation. The drug loading efficiency of CA@$CaCO_3$ NFs was observed to be 91% attained by the nanoencapsulation which depicts that $CaCO_3$ nanoparticles as a suitable porous carrier for the loading of hydrophobic drug citronellyl acetate. Fig. 2A illustrates the schematic representation for the fabrication of CA@$CaCO_3$ NFs from the synthesis of $CaCO_3$ nanoparticles using conch waste.

3.2.2. Swelling and drug release profiles of CA@$CaCO_3$ NFs

Drug release profiles depends on the swelling ratio, because, the drug release kinetics was initiated during swelling and surface erosion of the drug delivery carriers. In this study, swelling and drug release profiles of CA@$CaCO_3$ NFs were evaluated for every 3 h up to 24 h in the physiological pH (7.4). Initially in the first 3 h the wet weight based swelling ratio of CA@$CaCO_3$ NFs was 0.63 and it was gradually increased into 2.33 within 24 h. Whereas the swelling ratio was progressively increased every 3 h up to 24 h with the standard variation of 0.2 ± 0.09. The percentage of drug release for citronellyl acetate from CA@$CaCO_3$ NFs was observed to be found 31% on first 3 h and it was around 62% on 24

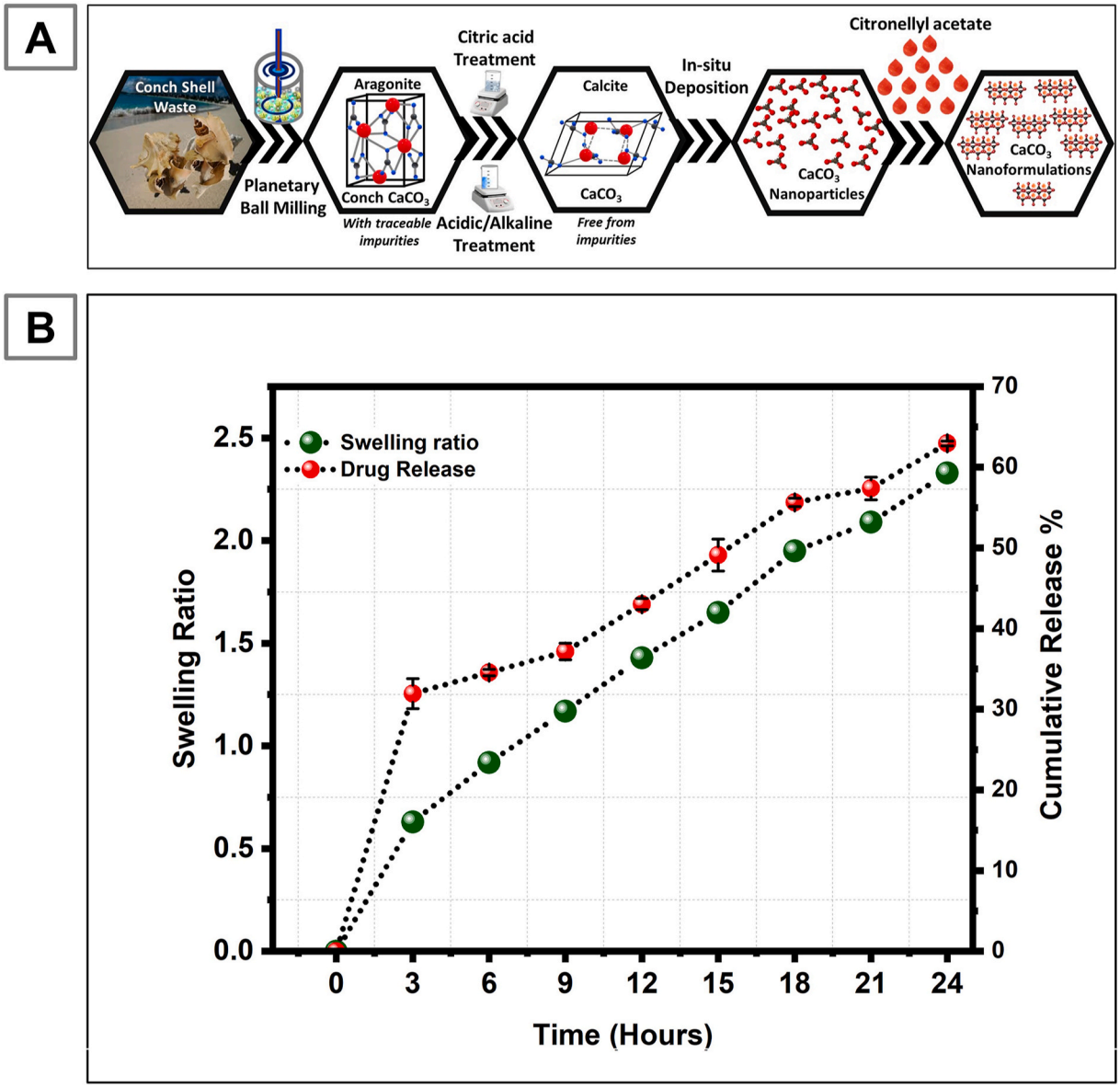

Fig. 2. (A)Schematic representation illustrates from synthesis of $CaCO_3$ nanoparticles using conch shell waste to fabrication of CA@$CaCO_3$ nanoformulations and (B) Swelling and drug release profiles of CA@$CaCO_3$ nanoformulations

h. During the first 3 intervals up to 9 h the drug release profile was evenly increased at the rate of 10%, after that release profile shows different increased percentage in order to the concentration of the citronellyl acetate released from the $CaCO_3$ nanoparticles. Anyhow the swelling and drug release profiles were corresponding each other because the percentage of drug release was increased, while the swelling ratio of CA@$CaCO_3$ NFs increased as shown in Fig. 2B.

3.3. UV–visible spectra

The UV–Visible absorption spectra of citronellyl acetate, $CaCO_3$ nanoparticles and CA@$CaCO_3$ NFs were recorded at 190 nm–800 nm. Citronellyl acetate alone exhibits the maximum absorption spectrum at 206 nm. Herein, $CaCO_3$ nanoparticles showed the absorption spectrum at 263 nm, which was similarly observed in CA@$CaCO_3$ NFs with reduced intensity (Ghadami Jadval Ghadam and Idrees, 2013). Incorporation of citronellyl acetate with $CaCO_3$ nanoparticles were the reasonable factor for decreased intensity in CA@$CaCO_3$ NFs. However, no predominant peak shift was observed between $CaCO_3$ nanoparticles and CA@$CaCO_3$ NFs (Fig. 3A).

3.4. FTIR spectra

The FTIR frequencies of citronellyl acetate shows the functional frequencies of 1023, 1454 and 3337 cm^{-1}corresponding to the stretching vibrations C–O groups and hydroxyl (-OH) groups. Besides to the above, the functional transmittance at around 1123 cm^{-1} specifically indicates the stretching vibrations of carbonyl (C═O) and C–O bonding of citronellol's ester derivative (Worzakowska, 2014). On other hand, functional frequencies of $CaCO_3$ nanoparticles and CA@$CaCO_3$ NFs shows functional frequencies at 709, 879 and 1447 cm^{-1} indicating the symmetrical and asymmetrical stretching vibrations of $CO_3^{2-}$of calcite $CaCO_3$ (Chavan et al., 2018). In the case of CA@$CaCO_3$ NFs the bending vibrations of calcite's CO_3^{2-} was specifically disrupted due to the incorporation of citronellyl acetate. Hence, it infers that citronellyl acetate (CA) was significantly loaded within the $CaCO_3$ nanoparticles as CA@$CaCO_3$ NFs (Fig. 3B).

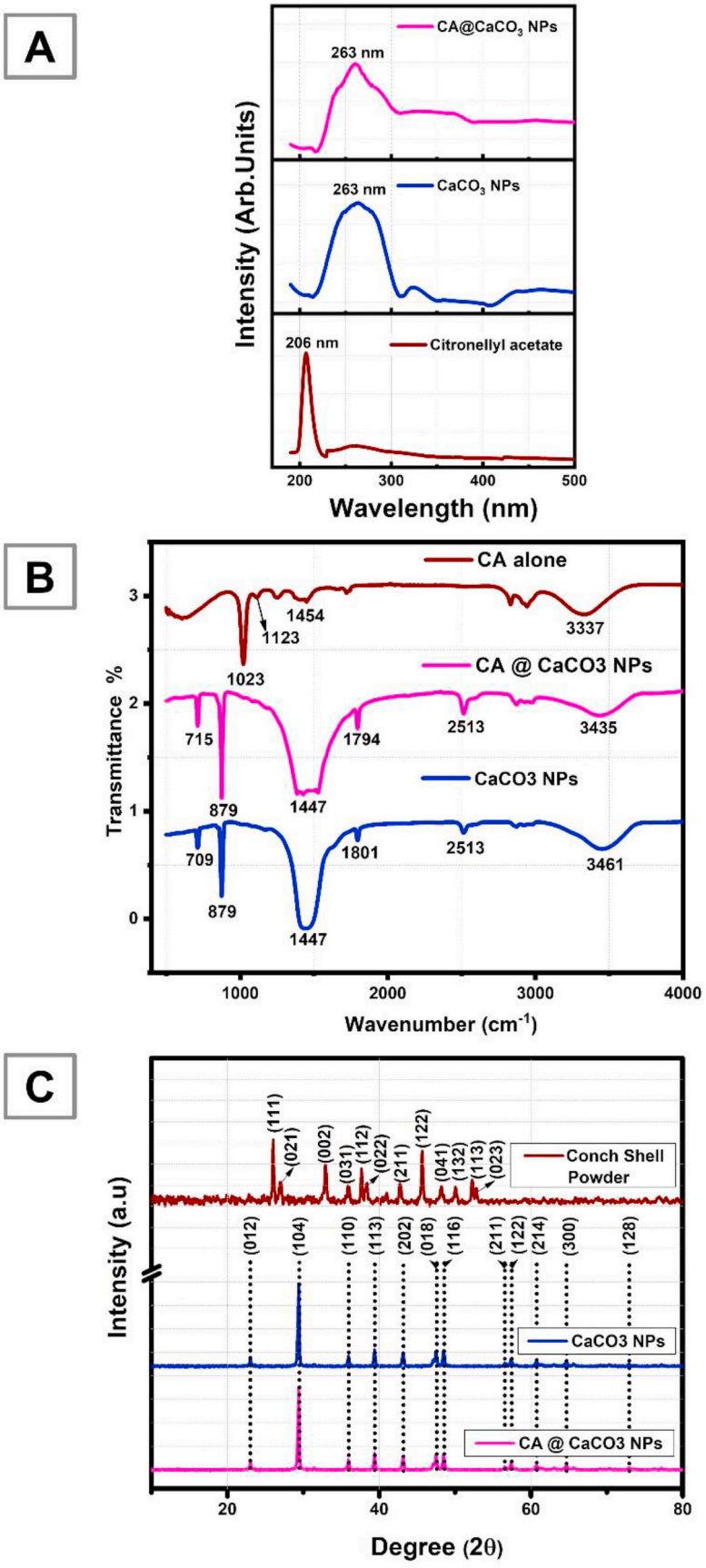

Fig. 3. (A) UV–Visible spectra of citronellyl acetate, $CaCO_3$ nanoparticles and CA@$CaCO_3$nanoformulations, (B) FTIR spectra of Citronellyl acetate, $CaCO_3$ nanoparticles and CA@$CaCO_3$ nanoformulations and (C) XRD pattern of conch shell powder, $CaCO_3$ nanoparticles and CA@$CaCO_3$ nanoformulations.

3.5. XRD pattern

XRD pattern of Ball milled conch powder exhibits the aragonite crystalline structure of $CaCO_3$ (JCPDS reference no: 41–1475). The aragonite phase of conch shell powder exhibits the hkl planes of (111), (021), (002), (031), (112), (022), (211), (122), (041), (132), (113) and (032) respectively for the 2θ values of 26.02, 26.99, 32.91, 35.89, 37.67, 38.38, 48.72, 45.67, 48.16, 50.10, 52.23 and 52.78 which originally defines aragonite orthorhombic crystal system. Aragonite phase is one of the metastable polymorphs of $CaCO_3$due to the presence of impurities and it has the probability to transverse into other polymorphs of $CaCO_3$ (Maleki Dizaj et al., 2015). XRD patterns of both $CaCO_3$ nanoparticles and CA@$CaCO_3$ NFs retains the similar rhombohedral calcite crystalline structure of $CaCO_3$ (JCPDS reference no: 00-005-0586) with the hkl planes of (012), (104), (110), (113), (202), (018), (116), (211), (122), (214), (300) and (128) respectively for the 2θ values of 23.13, 29.30, 35.98, 39.41, 43.22, 47.54, 48.56, 57.46, 60.67, 64.70 and 72.90. Calcite is the most stable form of $CaCO_3$, which has been obtained from the metastable aragonite crystal system by the elimination of impurities through calcination at 750 °C followed by step wise particle size reduction. Results reveal that stable calcite $CaCO_3$ nanoparticles synthesized from the conch shell powder and the incorporation of citronellyl acetate does not affect the calcite crystalline nature of $CaCO_3$ nanoparticles (Fig. 3C) (Chavan et al., 2018).

3.6. DLS spectra

Dynamic light scattering based on the Brownian motion has been utilized for the analysis of average particle size of $CaCO_3$ nanoparticles synthesized from conch powder in step wise manner and drug loaded nanoparticles as CA@$CaCO_3$ NFs (Fig. 4A). Particle size of raw conch shell $CaCO_3$ powder was observed to be 10.37 μm, which was reduced to 1.25 μm after ball milling resulting in the formation of $CaCO_3$. Citric acid treated $CaCO_3$ showed further reduction of size to 560 nm, which on alkaline: acidic treatment further reduced to 264 nm (Fig. S1), finally resulting in $CaCO_3$ nanoparticles of average size 59.2 nm through in-situ deposition method (Fig. 4A). When compared to $CaCO_3$ nanoparticles the average particle size of CA@$CaCO_3$ NFs increased to 142 nm, which might be due to loading of citronellyl acetate. Reports revealed that nanoparticles with size less ≤500 nm is suitable for the cellular uptake through the process endocytosis facilitating its penetration towards the physiological barriers like cell membrane and blood brain barrier (BBB) (Kumari and Yadav, 2011). Hence in the present study the $CaCO_3$ nanoparticles and CA@$CaCO_3$ NFs having size less than 500 nm is suitable for the treatment of CNS related disorder as it can penetrate through the BBB.

3.7. Morphological and elemental analyses

3.7.1. SEM and EDAX

The SEM morphology of $CaCO_3$ nanoparticles showed quasi spherical shaped calcite nanocrystals with dispersed arrangement of the particles. $CaCO_3$ nanoparticles with uniform morphology and size was obtained by step wise particle reduction of reinforced crystalline structure of conch $CaCO_3$. The present study involves loading of hydrophobic drug citronellyl acetate within $CaCO_3$ nanoparticles to overcome the draw backs of solubility of drug in biological fluids and permeability through BBB for neuroprotective applications. Citronellyl acetate loaded particles i.e., CA@$CaCO_3$ NFs exhibited agglomerated morphology into small clusters and the shape of the particles in CA@$CaCO_3$ NFs still retains in its spherical form. DLS spectra revealed that the size of the CA@$CaCO_3$ NFs as 142 nm suitable to transverse the blood brain barrier for the neuroprotective applications.

EDX analysis have been conducted for conch $CaCO_3$ and $CaCO_3$ nanoparticles respectively to determine the elemental composition of the samples. The major part on synthesis of $CaCO_3$ nanoparticles is to remove the organic and inorganic impurities present in the conch $CaCO_3$ to yield the purified $CaCO_3$ nanoparticles. EDX spectra of conch $CaCO_3$ showed the presence of carbon (C), calcium (Ca), and oxygen (O) in the weight percentage of 73.57%, 2.68% and 23.6% respectively. Inorganic impurities in the range of 0.05% of silicon (Si), 0.03% of manganese (Mn),0.04% of sodium (Na) and magnesium (Mg) was observed in the conch $CaCO_3$ source. EDX spectra of $CaCO_3$ nanoparticles synthesized through the step wise particle size reduction of conch $CaCO_3$ showed presence of Ca, C and O in the weight percentage of 21.63%, 17.40% and 60.97% respectively with no impurities as observed in conch shell $CaCO_3$. Remarkably the weight percentage of Ca was found to be 21.63% in synthesized $CaCO_3$ nanoparticles which is higher than the Ca weight percentage observed from conch $CaCO_3$ which is about 2.68%, ensuring step wise particle size reduction that significantly yield the increased Ca level in the sample by the removal of impurities. Calcination in every phase of step wise particle size reduction progressively eliminates the minor impurities present in the conch shell powder (Fig. 4B) (Savita et al., 2020).

3.7.2. TEM analysis

TEM micrograph(Fig. 4C) of calcite $CaCO_3$ nanoparticles randomly showed cubical and quasi spherical shaped particles in distinguished manner. Well dispersed shape of the $CaCO_3$ nanoparticles synthesized from the conch waste was observed, which might be due to removal of the contaminants and calcination process carried out during the step-wise particle size reduction. In the case of CA@$CaCO_3$ NFs slightly agglomerated clusters were observed without any change in shape, which might be due to incorporation of citronellyl acetate ensuring that drug loading factor does not affect the crystalline nature of the $CaCO_3$ nanoparticles as observed in XRD and SEM Results.

3.7.3. ICP – OES analysis

The ICP-OES analysis (Table 4) was carried out for the prediction of Ca (calcium) and other traceable elements including Cd (cadmium), Hg (mercury), Mg (magnesium), Pb (lead), Si (silicon), Zn (zinc) and As (arsenic) present in the conch $CaCO_3$ and synthesized $CaCO_3$ nanoparticles. Specific wavelength that identifies the elements in ICP –OES were Ca: 317.933 nm, Cd: 228.802 nm, Hg: 253.652 nm, Mg: 285.213 nm, Pb: 220.353 nm, Si: 251.611 nm, Zn: 213.857 nm and As: 188.979 nm. Elemental analysis of marine $CaCO_3$ matched with the MACS - 1 and MACS - 2 certified reference materials produced by USGS (United States Geological Survey). The ICP-OES analysis revealed the major constitution of Ca in the concentration of 29.07 μg/ml and 34.31 μg/ml respectively in conch $CaCO_3$ and $CaCO_3$ nanoparticles in ppm level. Also, the conch $CaCO_3$, showed the presence of Mg, Si and Zn in the minimum elemental compositions, which were reduced to less than 1 ppm in synthesized $CaCO_3$ nanoparticles. Moreover, the conch $CaCO_3$ showed the presence of Hg in the concentration of 0.134 μg/ml within the permissible level of exposure of Hg to the human being i.e. 1 ppm (Kumar and Puri, 2012), similarly in the synthesized $CaCO_3$ nanoparticles also the observed Hg level was below the detection limit. In both conch $CaCO_3$ and $CaCO_3$ nanoparticles heavy metals such as Cd, Pb and As were present below detection limit ensuring the biosafety level of $CaCO_3$ to human exposure. The major impurities present in the conch shell was removed or well minimized in synthesized $CaCO_3$ nanoparticles due to the progress of step wise particle size reduction.

3.8. Neuroprotective evaluation

An in-silico high-throughput screening is an advantageous platform for identification of effective pharmaceutical agents and virtual screening reduces the time and cost utilized for the invention of drugs. In the present study, plant polyphenolic derivative (Karanjin) was evaluated for its neuroprotective potential through in-silico molecular docking with protein-ligand complexes of markers of Alzheimer's and Parkinson's diseases (Durán-Iturbide et al., 2020; Gnanaraj et al., 2022).

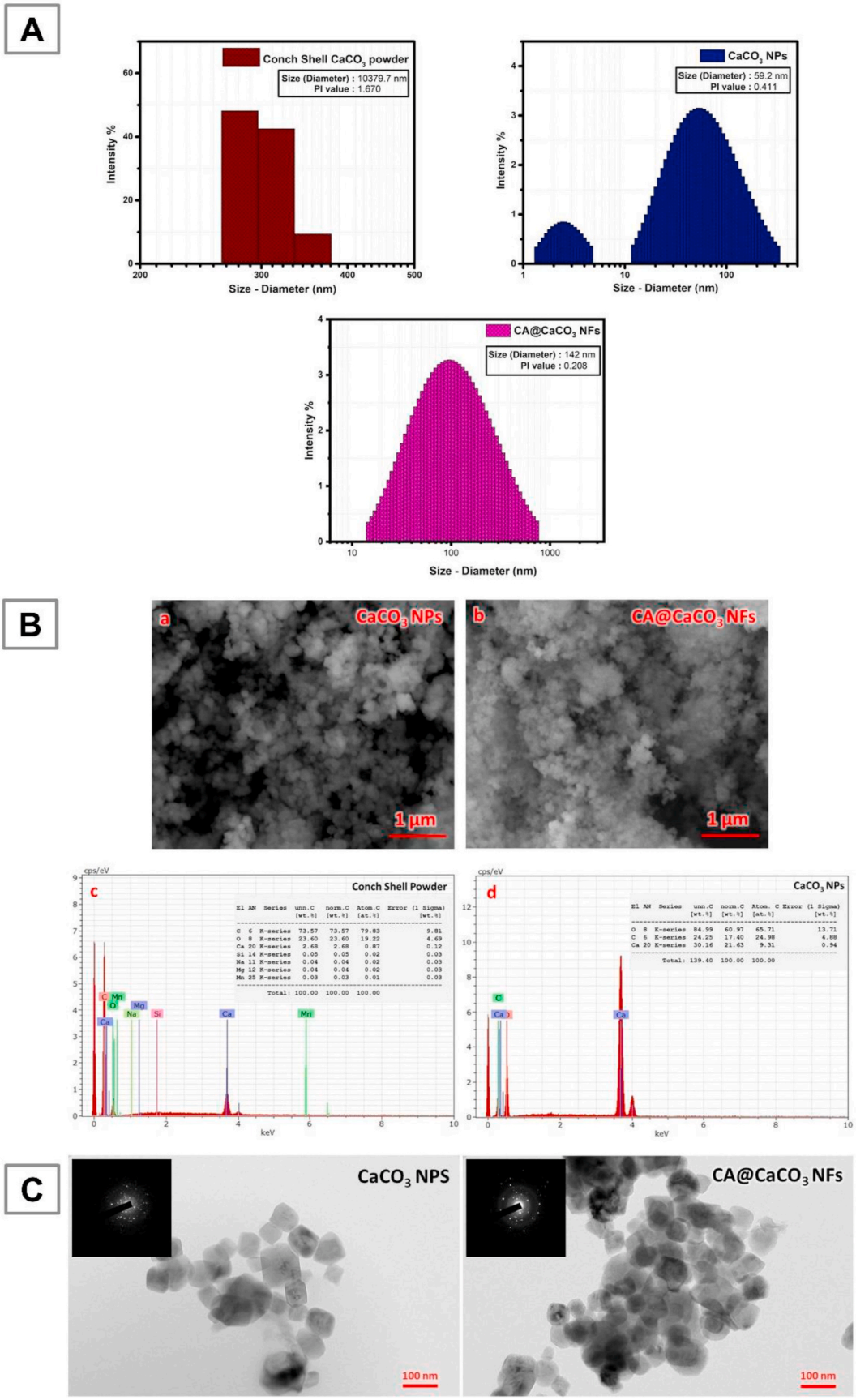

Fig. 4. (A) DLS spectra of conch shell $CaCO_3$ powder, $CaCO_3$ nanoparticles and CA@$CaCO_3$ nanoformulations, (B - a and b) SEM images of $CaCO_3$ nanoparticles and CA@$CaCO_3$ nanoformulations, (B - c and d) EDX spectra of conch shell $CaCO_3$ powder and $CaCO_3$ nanoparticles and (C) TEM and SAED pattern of $CaCO_3$ nanoparticles and CA@$CaCO_3$ nanoformulations.

Table 4
Elemental composition level of $CaCO_3$ determined by ICP-OES.

Sample	Elements	Dilution Factor	Concentration in ppm µg/ml
Conch $CaCO_3$	Calcium **(Ca)**	100	29.07
	Cadmium **(Cd)**		BDL
	Mercury **(Hg)**		0.134
	Magnesium **(Mg)**		4.071
	Lead **(Pb)**		BDL
	Silicon **(Si)**		3.105
	Zinc **(Zn)**		5.756
	Arsenic**(As)**		BDL
$CaCO_3$ nanoparticles	Calcium **(Ca)**		34.21
	Cadmium **(Cd)**		BDL
	Mercury **(Hg)**		BDL
	Magnesium **(Mg)**		0.073
	Lead **(Pb)**		BDL
	Silicon **(Si)**		0.097
	Zinc **(Zn)**		0.826
	Arsenic **(As)**		BDL

BDL - Below detection limit

Likewise, we selected the citronellyl acetate as a source of neuroprotective agent through in-silico high-throughput screening based on the highest docking score on ADMET (absorption, distribution, metabolism, excretion and toxicity) evaluation. Since there are drawbacks on neuroprotective agents including the permeability on BBB, blood - CSF barrier and the sensitivity of the neuroprotective agents with respect to the environmental and human physiological factors such as pH, temperature and oxidation. To overcome these drawbacks, immobilization of neuroprotective agents was suggested with a suitable nanocarrier system for sustained drug release and enhanced bioavailability. The antioxidant phenomenon exhibited significant neuroprotective potential by neutralising the free radicals responsible for oxidative stress leading to neuronal dysfunction. Hence, this work plan assessed the antioxidant, AChE inhibition and Aβ anti/disaggregation profiles of the neuroprotective drug citronellyl acetate (selected through in-silico high throughput screening), $CaCO_3$ nanoparticles and CA@$CaCO_3$ NFs.

3.8.1. *Free radical scavenging assay*

Multiple evidences revealed that oxidative stress played pivotal role in the degeneration of neurons leading to cognitive dysfunction in AD (Butterfield and Halliwell, 2019; Cassidy et al., 2020). Based on these reports the antioxidant potential of $CaCO_3$ nanoparticles and CA@$CaCO_3$ NFs were analysed using DPPH radical scavenging assay. Citronellyl acetate, $CaCO_3$ nanoparticles and CA@$CaCO_3$ NFs showed dose dependant increase in free radical scavenging activity with 89%, 42% and 90% radical scavenging activity at the maximum dose of 50 µg/ml respectively in 1 h incubation (Fig. 5-A1). IC_{50} value of citronellyl acetate, $CaCO_3$ nanoparticles and CA@$CaCO_3$ NFs were observed to be 27.17 ± 1.342, 25.55 ± 0.93 and 29.27 ± 2.6 µg/ml respectively. DPPH scavenging assay with 2 h incubation exhibited scavenging activity of 63%, 48% and 92% respectively at its maximum dose with the IC_{50} value of 37.27 ± 11.42, 23.68 ± 0.19l and 41.51 ± 0.69 µg/ml (Fig. 5A2) for citronellyl acetate, $CaCO_3$ nanoparticles and CA@$CaCO_3$ NFs. Percentage of free radical scavenging for citronellyl acetate were reduced from 89% in first 60 min incubation to 63% in 120 min incubation which

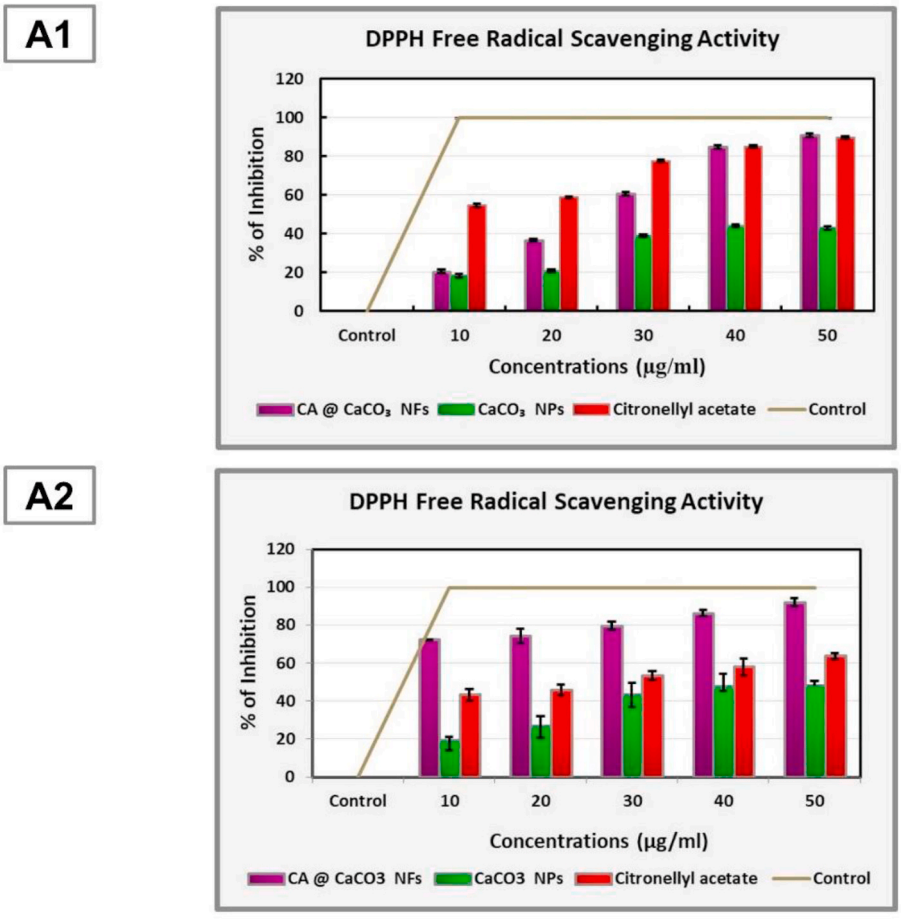

Fig. 5. (A1) DPPH free radical scavenging of citronellyl acetate, $CaCO_3$and nanoparticles CA@$CaCO_3$ nanoformulations under 1-h incubation; (A2) DPPH free radical scavenging of citronellyl acetate, $CaCO_3$ nanoparticles and CA@$CaCO_3$ nanoformulations under 2 h of incubation.

might be due to sensitivity of citronellyl acetate to certain parameters such as temperature, oxidation, light, moisture and the digestive systems (Rostami et al., 2019). However CA@$CaCO_3$ NFs showed increased free radical scavenging activity (92.2%) in 120 min than 60 min incubation (90.77%), when compared to citronellyl acetate and $CaCO_3$ nanoparticles alone. Higher antioxidant potential of CA@$CaCO_3$ NFs on DPPH free radical scavenging might be due to the following reasons the (i) synergistic antioxidant potential of citronellyl acetate and $CaCO_3$ nanoparticles, (ii) protection of citronellyl acetate from the sensitive parameters and (iii) sustained release of citronellyl acetate by $CaCO_3$ nanoparticles (Pateiro et al., 2021).

3.8.2. *Acetylcholinesterase inhibition assay*

Lack of choline acetyl transferase the key enzyme involved in the synthesis of acetylcholine (ACh) leads to loss of neurotransmission due to reduction of ACh as it is degraded by AChE which leads to the degeneration of cholinergic neurons causing neurodegeneration in AD (Sharma, 2019). AChE has been implicated in the pathogenesis of AD as AChE directly interacts with Aβ peptide promoting its aggregation to insoluble plaques. Reports have revealed that AChE has cross talks with Aβ and hyper-phosphorylated tau protein, hence AChE inhibition modulates the processing of APP and protects the neurons against various insults (García-Ayllón et al., 2011; Marucci et al., 2021). Hence the present work focuses on inhibition of AChE for the treatment of AD. Results revealed that citronellyl acetate, $CaCO_3$ nanoparticles and CA@$CaCO_3$ NFs showed potent AChE inhibition in a dose dependent manner (Fig. 6). At the highest concentration of 50 μg/ml the citronellyl acetate, $CaCO_3$ nanoparticles,CA@$CaCO_3$ NFs and Donepezil (positive control) exhibited the percentage of AChE inhibition e 92 %, 57%, 95% and 84% respectively, with the IC_{50} value of 26.54 ± 2.54, 30.62 ± 4.1, 25.62 ± 1.5 and24.799 ± 0.62 μg/ml. Comparatively, CA@$CaCO_3$ NFs showed highest percentage of AChE inhibition than citronellyl acetate and $CaCO_3$ nanoparticles. Interestingly, CA@$CaCO_3$ NFs showed increased AChE inhibitory potential when compared to the positive control which ensures that CA@$CaCO_3$ NFs were the suitable drug delivery system for AD treatment.

3.8.3. *Aβ anti-aggregation and disaggregation studies*

The abnormal misfolding and aggregation of Aβ peptide accelerated the formation of amyloid plaques and neurofibrillary tangles (NFTs), which triggers oxidative stress neuronal death in Alzheimer's and Parkinson's disorders. Therefore, researchers focused on the invention of nutraceuticals and their encapsulant forms to sustain the averting behavior of Aβ peptide aggregation. To attenuate the aggregation and misfolding of Aβ peptide, the plant phytochemicals and their derivatives were encapsulated with the nanoparticles as a carrier system for the purpose of enhanced neuroprotection (Pugazhendhi et al., 2018; Prakashkumar et al., 2021). In this work, the ability of citronellyl acetate, $CaCO_3$ nanoparticles and CA@$CaCO_3$ NFs were assessed against the aggregation and fibril formation of Aβ peptide by using Th-T assay. Th-T is an intercalating dye that binds between the Aβ fibrils was used to determine the Aβ peptide aggregation.

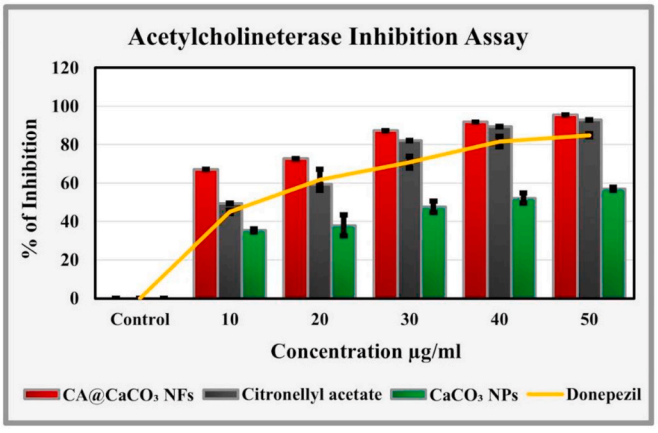

Fig. 6. AChE inhibition of citronellyl acetate, $CaCO_3$ and nanoparticles and CA@$CaCO_3$ nanoformulations

The sigmoidal curve (Fig. 7A) represents the increase in fluorescence intensity of Aβ peptide from monomers (0h) to fibrils of oligomers (48 h) and matured plaques (96 h) in time dependant manner in comparison with Th-T blank. Th-T intercalates within Aβ fibrils and its fluorescent intensity increases with increase in fibrillation process in time dependant manner. Results revealed the formation of fibrils and plaques from Aβ monomeric peptide at physiological pH (7.4).

The desired concentration 40 μg/ml of citronellyl acetate, $CaCO_3$ nanoparticles, CA@$CaCO_3$ NFs and galantamine (positive control) incubated with Aβ peptide showed noticeable reduction in fluorescent intensities of Th-T when compared to the Aβ peptide alone which represents the defibrillation phenomenon of the above samples. Phase I studies were carried out to evaluate the antiaggregation potential of Aβ peptide from 0 to 20 h and 48 h in the presence and absence of citronellyl acetate, $CaCO_3$ nanoparticles, CA@$CaCO_3$ NFs and galantamine. Results of phase I (Fig. 7B) showed 5-fold and 12-fold increase in fluorescent intensities in control group (Aβ) alone) in 20 h (130.66 ± 5.391 a.u.) and 48 h (321.66 ± 9.309 a.u.) respectively, in comparison to 0 h (25 ± 1.788) which substantiate the formation of oligomers from monomers at 20 h and protofibrils in 48 h. Whereas, the CA@$CaCO_3$ NFs shows the 2-fold (80 ± 4.472 a.u.) and 3-fold (118.33 ± 6.831 a.u.) reduction in Th-T fluorescent intensities in 20 h and 48 h respectively, when compared to Aβ peptide alone. CA@$CaCO_3$ NFs showed potent decrease in fluorescent intensity than citronellyl acetate and $CaCO_3$ nanoparticles, but similar to positive control galantamine which showed 2-fold reduction in fluorescent intensity in 20 h and 48 h. Fluorescent microscopic images showed the presence of bright green fluorescence in Aβ peptide control, while treated samples showed significant reduction in fluorescent intensity substantiating the results of spectrofluorimetry (Fig. 8). Results depicted the fact that CA@$CaCO_3$ NFs effectively attenuated the aggregation of Aβ peptide.

Phase II studies were carried out to assess the defibrillization effect of CA@$CaCO_3$ NFs. Briefly, Aβ plaques formed in 96 h were treated with 40 μg/ml of citronellyl acetate, $CaCO_3$ nanoparticles, CA@$CaCO_3$ NFs and galantamine to evaluate the disaggregation ability. CA@$CaCO_3$ NFs showed (Fig. 7C) fluorescent intensity of 201.66 ± 6.831 a.u. Which is 3-fold lower than the fluorescent intensity of Aβ plaques alone (585 ± 11.832 a.u.) at 96 h. Fluorescent intensity for CA@$CaCO_3$ NFs was observed to be two-fold lesser (297 ± 5.440 a.u.) when compared to fluorescent intensity of Aβ plaques alone (706.33 ± 10.595) in 9 days. Microscopic observation confirmed the results of spectrofluorimeter revealing the fact that CA@$CaCO_3$ NFs disaggregates Aβ mature fibrils and prevents the formation of mature plaques when compared to vehicle control (Fig. 8). Overall results of the present study reveal that CA@CO_3 NFs acts as potent neuroprotectant via its antioxidant, acetyl cholinesterase inhibition, antiamyloidogenic effect (i.e.antiaggreagation and disaggregation ability. (Figs. 7 and 8).

4. Conclusion

The synthesis of $CaCO_3$ nanoparticles from marine waste results in eco-friendly, cost effective and waste management approach. The XRD pattern confirms the crystalline phase transition of $CaCO_3$ from metastable aragonite form of conch $CaCO_3$ to stable calcite form of synthesized $CaCO_3$ nanoparticles. EDX and ICP-OES results revealed the presence of impurity elements in marine waste conch $CaCO_3$, while synthesized $CaCO_3$ nanoparticles exhibited less than 1 ppm impurities ensuring its biosafety level in drug delivery applications. Sustained drug release, protection of drug citronellyl acetate from physiological parameters and enhanced antioxidant, AChE inhibition and

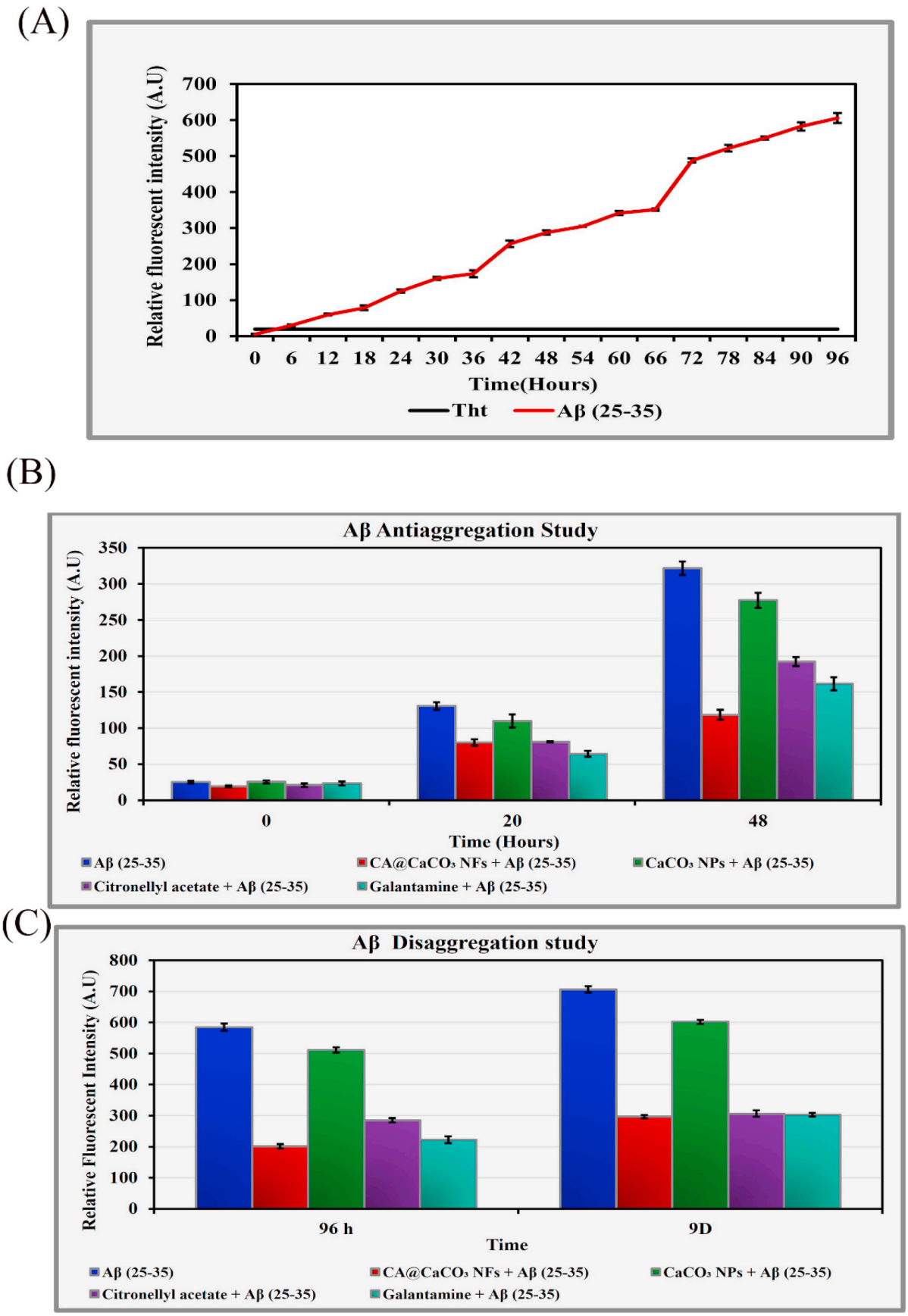

Fig. 7. (A) Sigmoidal curve of fluorescent intensity for Aβ peptidefrom monomers to mature fibrils and Th-T alone; (B)Th-T fluorescent assay representsAβ peptide antiaggregation effect of citronellyl acetate, $CaCO_3$nanoparticles and CA@$CaCO_3$ nanoformulations; (C)Th-T fluorescent assay representsAβ peptide disaggregation effect of citronellyl acetate, $CaCO_3$nanoparticles and CA@$CaCO_3$ nanoformulations.

antiamyloidogenic effect of CA@CO_3 NFs revealed the fact that $CaCO_3$ nanoparticle is the suitable nanocarrier for the delivery of neuroprotective drug citronellyl acetate. Hence, the CA@CO_3 NFs fabricated by the incorporation of marine waste derived $CaCO_3$ nanoparticles and citronellyl acetate selected through *in-silico* high throughput screening acts as potent neuroprotective agent for the treatment of AD and other neurodegenerative disorders like Parkinson's disease.

Credit author statement

Nallasamy Prakashkumar - Conceptualization, Methodology, Formal analysis, Data curation, Software, Investigation, Writing-original draft, Visualization; **Beema Shafreen Rajamohamed –** Formal analysis and software investigation; **Jeyakanthan Jeyaraman** – Review & Editing; **Brindhadevi Kathirvel –** Review and editing**; Natarajan Suganthy -** Review & Editing, Supervision.

Declaration of competing interest

The authors declare that they have no known competing financial interests or personal relationships that could have appeared to influence the work reported in this paper.

Data availability

The data that has been used is confidential.

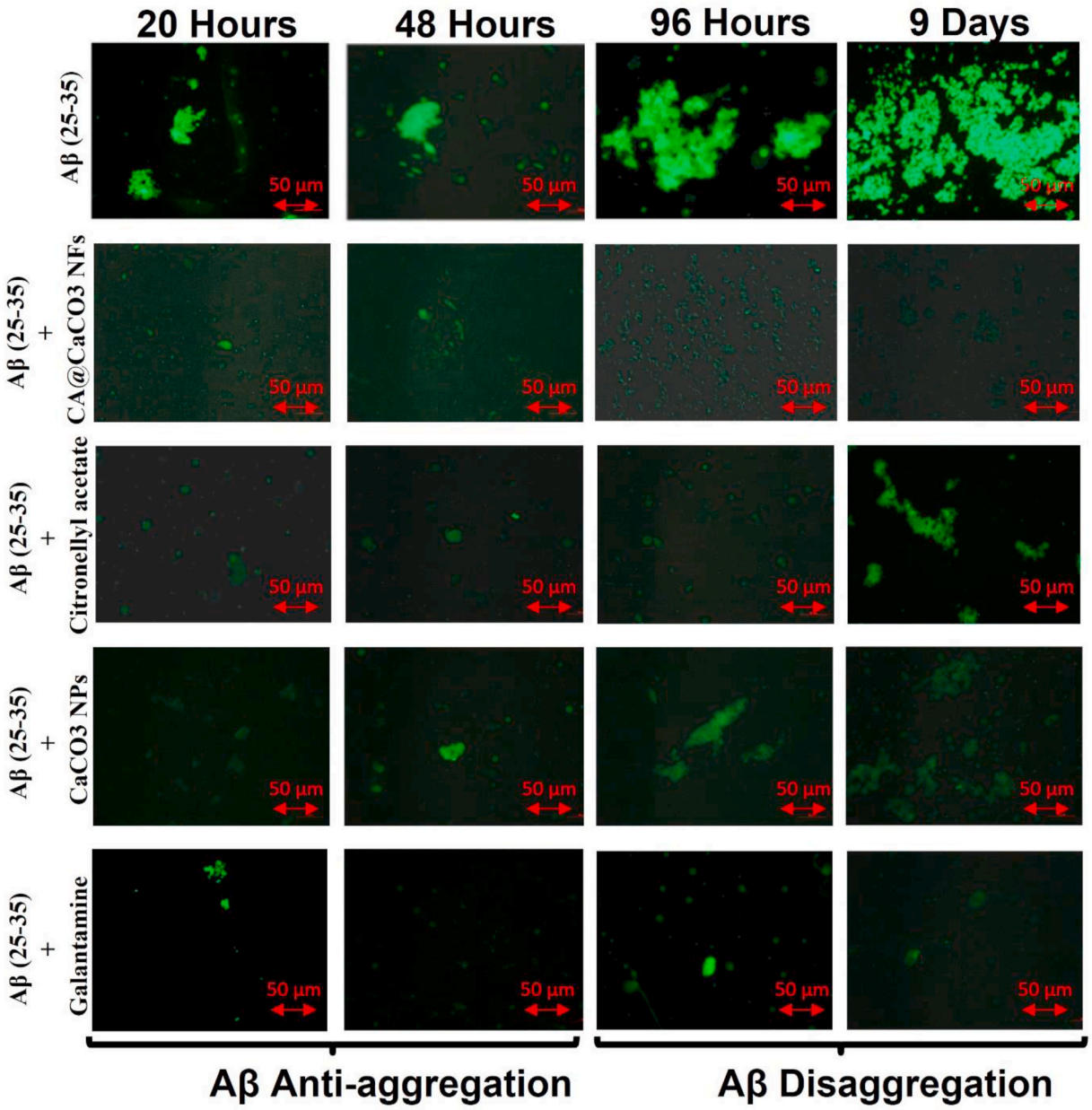

Fig. 8. Fluorescent microscope images of Aβ peptide antiaggregation and disaggregation for citronellyl acetate, $CaCO_3$nanoparticles and CA@$CaCO_3$ nanoformulations

Acknowledgment

N.Suganthy and N. Prakashkumar thank the RUSA-Phase 2.0 grant (No. F. 24-51/2014-U, Policy (TN Multi-Gen), Dept. of Edn. Govt.of India, (Dated: 09.10.2018).Authors also acknowledge the Department of Science and Technology, New Delhi for the financial support in general and infrastructure facilities sponsored under PURSE 2nd Phase programme (Order No. SR/PURSE Phase 2/38 (G) dated:21.02.2017).

Appendix A. Supplementary data

Supplementary data to this article can be found online at https://doi.org/10.1016/j.envres.2023.115631.

References

Ali Said, F., Bousserrhine, N., Alphonse, V., Michely, L., Belbekhouche, S., 2020. Antibiotic loading and development of antibacterial capsules by using porous CaCO3 microparticles as starting material. Int. J. Pharm. 579, 119175 https://doi.org/10.1016/j.ijpharm.2020.119175.

Benny, A., Thomas, J., 2019. Essential oils as treatment strategy for alzheimer's disease: current and future perspectives. Planta Med. 85 (3), 239–248. https://doi.org/10.1055/a-0758-0188.

Breijyeh, Z., Karaman, R., 2020. Comprehensive review on Alzheimer's disease: causes and treatment. Molecules 25, 5789. https://doi.org/10.3390/molecules25245789.

Butterfield, D.A., Halliwell, B., 2019. Oxidative stress, dysfunctional glucose metabolism and Alzheimer disease. Nature reviews. Neuroscience 20 (3), 148–160. https://doi.org/10.1038/s41583-019-0132-6.

Cassidy, L., Fernandez, F., Johnson, J.B., Naiker, M., Owoola, A.G., Broszczak, D.A., 2020. Oxidative stress in alzheimer's disease: a review on emergent natural polyphenolic therapeutics. Compl. Ther. Med. 49, 102294 https://doi.org/10.1016/j.ctim.2019.102294.

Chavan, S., Tayade, S., Gupta, V., Deshmukh, V., Sardeshmukh, S., 2018. Pharmaceutical standardization and physicochemical characterization of traditional ayurvedic marine drug: incinerated conch shell (Shankha Bhasma). Mar. Drugs 16 (11). https://doi.org/10.3390/md16110450.

Dizaj, S.M., Barzegar-Jalali, M., Hossein Zarrintan, M., Adibkia, K., Lotfipour, F., 2015. Calcium carbonate nanoparticles; Potential in bone and tooth disorders. Pharmaceut. Sci. 20 (4), 175–182. https://doi.org/10.5681/PS.2015.008.

Durán-Iturbide, N.A., Díaz-Eufracio, B.I., Medina-Franco, J.L., 2020. In silico ADME/tox profiling of natural products: a focus on BIOFACQUIM. ACS Omega 5 (26), 16076–16084. https://doi.org/10.1021/acsomega.0c01581.

García-Ayllón, M.S., Small, D.H., Avila, J., Sáez-Valero, J., 2011. Revisiting the role of acetylcholinesterase in alzheimer's disease: cross-talk with P-tau and β-amyloid. Front. Mol. Neurosci. 4, 22. https://doi.org/10.3389/fnmol.2011.00022.

Ghadami Jadval Ghadam, A., Idrees, M., 2013. Characterization of $CaCO_3$ nanoparticles synthesized by reverse microemulsion technique in different concentrations of surfactants. Iran. J. Chem. Chem. Eng. (Int. Engl. Ed.) 32 (3), 27–35.

Gnanaraj, C., Sekar, M., Fuloria, S., Swain, S.S., Gan, S.H., Chidambaram, K., Rani, N.N.I. M., Balan, T., Stephenie, S., Lum, P.T., Jeyabalan, S., Begum, M.Y., Chandramohan, V., Thangavelu, L., Subramaniyan, V., Fuloria, N.K., 2022. Silico molecular docking analysis of karanjin against alzheimer's and Parkinson's diseases as a potential natural lead molecule for New drug design, development and therapy. Molecules 27 (9), 2834. https://doi.org/10.3390/molecules27092834.

Hariharan, Manjusha, Varghese, Neethumol, Benny Cherian, A., Sreenivasan, P.V., JenishPaul, Asmy Antony, K.A., 2014. Synthesis and characterisation of CaCO3 (calcite) NanoParticles from cockle shells using chitosan as precursor. Int. J. Scientific Res. Publications 4, 1–5.

Hussain, B., Fang, C., Chang, J., 2021. Blood-brain barrier breakdown: an emerging biomarker of cognitive impairment in normal aging and dementia. Front. Neurosci. 15, 688090 https://doi.org/10.3389/fnins.2021.688090.

Hussein, A.I., Ab-Ghani, Z., Mat, A.N.C., Ghani, N.A.A., Husein, A., Rahman, I.A., 2020. Synthesis and characterization of spherical calcium carbonate nanoparticles derived from cockle shells. Appl. Sci. 10 (20), 1–14. https://doi.org/10.3390/app10207170.

Ingkaninan, K., de Best, C.M., van der Heijden, R., Hofte, A.J., Karabatak, B., Irth, H., Tjaden, U.R., van der Greef, J., Verpoorte, R., 2000. High-performance liquid chromatography with on-line coupled UV, mass spectrometric and biochemical detection for identification of acetylcholinesterase inhibitors from natural products. J. Chromatogr. A 872 (1–2), 61–73. https://doi.org/10.1016/s0021-9673(99)01292-3.

Ingle, S.V., Joshi, K.A., 2017. Exploring quantum chemical descriptors and molecular docking approach for designing antagonist search model for the Glycine/NMDA receptor site. ChemistrySelect 2 (32), 10476–10483. https://doi.org/10.1002/slct.201702291.

Khurana, R., Coleman, C., Ionescu-Zanetti, C., Carter, S.A., Krishna, V., Grover, R.K., Roy, R., Singh, S., 2005. Mechanism of thioflavin T binding to amyloid fibrils. J. Struct. Biol. 151 (3), 229–238. https://doi.org/10.1016/j.jsb.2005.06.006.

Kumar, M., Puri, A., 2012. A review of permissible limits of drinking water. Indian J. Occup. Environ. Med. 16 (1), 40–44. https://doi.org/10.4103/0019-5278.99696.

Kumari, A., Yadav, S.K., 2011. Cellular interactions of therapeutically delivered nanoparticles. Expet Opin. Drug Deliv. 8 (2), 141–151. https://doi.org/10.1517/17425247.2011.547934.

Li, J., Jiang, H., Ouyang, X., Han, S., Wang, J., Xie, R., Zhu, W., Ma, N., Wei, H., Jiang, Z., 2016. $CaCO_3$/Tetraethylenepentamine-Graphene hollow microspheres as biocompatible bone drug carriers for controlled release. ACS Appl. Mater. Interfaces 8 (44), 30027–30036. https://doi.org/10.1021/acsami.6b10697.

Mailafiya, M.M., Abubakar, K., Chiroma, S.M., Danmaigoro, A., Zyoud, T.Y.T., Rahim, E. B.A., Zakaria, Z.A.B., 2022. Curcumin-loaded cockle shell-derived calcium carbonate nanoparticles ameliorates lead-induced neurotoxicity in rats via attenuation of oxidative stress. Food Sci. Nutr. https://doi.org/10.1002/fsn3.3096.

Maleki Dizaj, S., Barzegar-Jalali, M., Zarrintan, M.H., Adibkia, K., Lotfipour, F., 2015. Calcium carbonate nanoparticles as cancer drug delivery system. Expet Opin. Drug Deliv. 12 (10), 1649–1660. https://doi.org/10.1517/17425247.2015.104953.

Martín-Rapun, R., De Matteis, L., Ambrosone, A., Garcia-Embid, S., Gutierrez, L., de la Fuente, J.M., 2017. Targeted nanoparticles for the treatment of alzheimer's disease. Curr. Pharmaceut. Des. 23 (13), 1927–1952. https://doi.org/10.2174/1381612822666161226151011.

Marucci, G., Buccioni, M., Ben, D.D., Lambertucci, C., Volpini, R., Amenta, F., 2021. Efficacy of acetylcholinesterase inhibitors in Alzheimer's disease. Neuropharmacology 190, 108352. https://doi.org/10.1016/j.neuropharm.2020.108352.

Moreno, L.C.G.E.I., Puerta, E., Suárez-Santiago, J.E., Santos-Magalhães, N.S., Ramirez, M.J., Irache, J.M., 2017. Effect of the oral administration of nanoencapsulated quercetin on a mouse model of Alzheimer's disease. Int. J. Pharm. 517 (1–2), 50–57. https://doi.org/10.1016/j.ijpharm.2016.11.061.

National Center for Biotechnology Information, 2022. PubChem Compound Summary for CID 10340, Sodium Carbonate. Retrieved May 29, 2022 from. https://pubchem.ncbi.nlm.nih.gov/compound/Sodium-carbonate.

Ovais, M., Zia, N., Ahmad, I., Khalil, A.T., Raza, A., Ayaz, M., et al., 2018. Phyto-therapeutic and nanomedicinal approaches to cure Alzheimer's disease: present status and future opportunities. Front. Aging Neurosci. 10 https://doi.org/10.3389/fnagi.2018.00284.

Pateiro, M., Gómez, B., Munekata, P.E.S., Barba, F.J., Putnik, P., Kovačević, D.B., Lorenzo, J.M., 2021. Nanoencapsulation of promising bioactive compounds to improve their absorption, stability, functionality and the appearance of the final Food products. Molecules 26 (2021), 1547. https://doi.org/10.3390/molecules26061547.

Pires, D.E., Blundell, T.L., Ascher, D.B., 2015. pkCSM: predicting small-molecule pharmacokinetic and toxicity properties using graph-based signatures. J. Med. Chem. 58 (9), 4066–4072. https://doi.org/10.1021/acs.jmedchem.5b00104.

Prakashkumar, N., Thenmozhi, R., Thajuddin, N., Rajasree, S., Pugazhendhi, A., Suganthy, N., 2020. Polyherbal drug loaded starch nanoparticles as promising drug delivery system: antimicrobial, antibiofilm and neuroprotective studies. Process Biochem. 92, 355–364. https://doi.org/10.1016/j.procbio.2020.01.026.

Prakashkumar, N., Sivamaruthi, B.S., Chaiyasut, C., Suganthy, N., 2021. Decoding the neuroprotective potential of methyl gallate-loaded starch nanoparticles against beta amyloid-induced oxidative stress-mediated apoptosis: an in vitro study. Pharmaceutics 13 (3), 299. https://doi.org/10.3390/pharmaceutics13030299.

Pugazhendhi, A., Beema Shafreen, R., Pandima Devi, K., Suganthy, N., 2018. Assessment of antioxidant, anticholinesterase and antiamyloidogenic effect of Terminalia chebula, Terminalia arjuna and its bioactive constituent 7-Methyl gallic acid – an in vitro and in silico studies. J. Mol. Liq. 257, 69–81. https://doi.org/10.1016/j.molliq.2018.02.081.

Render, D., Samuel, T., King, H., Vig, M., Jeelani, S., Babu, R.J., Rangari, V., 2016. Biomaterial-derived calcium carbonate nanoparticles for enteric drug delivery. J. Nanomater. 2016 https://doi.org/10.1155/2016/317024.

Rostami, M.R., Yousefi, M., Khezerlou, A., Mohammadi, M.A., Jafari, S.M., 2019. Application of different biopolymers for nanoencapsulation of antioxidants via electrohydrodynamic process. Food Hydrocolloids. https://doi.org/10.1016/j.foodhyd.2019.06.015.

Saleh, S.R., Abady, M.M., Nofal, M., Yassa, N.W., Abdel-Latif, M.S., Nounou, M.I., Ghareeb, D.A., Abdel-Monaem, N., 2021. Berberine nanoencapsulation attenuates hallmarks of scoplomine induced alzheimer's-like disease in rats. Curr. Rev. Clin. Experiment. Pharmacol. 16 (2), 139–154. https://doi.org/10.2174/1574884715666200628112844.

Savita, S., Yadevedra, Y., Usha, S., Sushma, R., Khemchand, S., 2020. Characterization of conch shell nanoparticles (shanka bhasma) synthesized by the classical method. Scholars Int. J. Traditional and Complementary Med. 3 (5), 90–99. https://doi.org/10.36348/sijtcm.2020.v03i05.002.

Scuteri, D., Morrone, L.A., Rombolà, L., Avato, P.R., Bilia, A.R., Corasaniti, M.T., Sakurada, S., Sakurada, T., Bagetta, G., 2017. Aromatherapy and aromatic plants for the treatment of behavioural and psychological symptoms of dementia in patients with alzheimer's disease: clinical evidence and possible mechanisms. Evid. base Compl. Alternative Med.: eCAM 2017, 9416305. https://doi.org/10.1155/2017/9416305.

Seong, S.H., Paudel, P., Jung, H.A., Choi, J.S., 2019. Identifying phlorofucofuroeckol-A as a dual inhibitor of amyloid-β25-35 self-aggregation and insulin glycation: elucidation of the molecular mechanism of action. Mar. Drugs 17 (11), 600. https://doi.org/10.3390/md17110600.

Sharma, K., 2019. Cholinesterase inhibitors as Alzheimer's therapeutics (Review). Mol. Med. Rep. 20 (2), 1479–1487. https://doi.org/10.3892/mmr.2019.10374.

Silva, M.V.F., Loures, C.M.G., Alves, L.C.V., de Souza, L.C., Borges, K.B.G., Carvalho, M. D.G., 2019. Alzheimer's disease: risk factors and potentially protective measures. J. Biomed. Sci. 26 (1), 33. https://doi.org/10.1186/s12929-019-0524-y.

Trushina, D.B., Borodina, T.N., Belyakov, S., Antipina, M.N., 2022. Calcium Carbonate Vaterite Particles for Drug Delivery: Advances and Challenges. Materials Today Advances. Elsevier Ltd. https://doi.org/10.1016/j.mtadv.2022.100214.

Weller, J., Budson, A., 2018. Current understanding of Alzheimer's disease diagnosis and treatment. F1000Research, 7, F1000 *Faculty Rev*-1161. https://doi.org/10.12688/f1000research.14506.1.

Worzakowska, M., 2014. Thermal properties of citronellyl diesters. J. Therm. Anal. Calorimetry 118 (1), 299–309. https://doi.org/10.1007/s10973-014-3945-6.

Zhao, P., Tian, Y., Lu, Y., et al., 2022. Biomimetic calcium carbonate nanoparticles delivered IL-12 mRNA for targeted glioblastoma sono-immunotherapy by ultrasound-induced necroptosis. J. Nanobiotechnol. 20, 525. https://doi.org/10.1186/s12951-022-01731-z.

World Health Organization (WHO), 2022. A fact sheet about Dementia. https://www.who.int/news-room/fact-sheets/detail/dementia.